

# Control Mechanisms of Photoisomerization in Protonated Schiff Bases

Lela Vuković<sup>1,2</sup>, Carl F. Burmeister<sup>1</sup>, Petr Král<sup>2,3</sup>, Gerrit  
Groenhof<sup>1,4</sup>

<sup>1</sup>Department of Theoretical and Computational Biophysics, Max Planck Institute for Biophysical Chemistry, Am Fassberg 11, D-37077 Göttingen, Germany

<sup>2</sup>Department of Chemistry, University of Illinois at Chicago, Chicago, IL 60607, United States

<sup>3</sup>Department of Physics, University of Illinois at Chicago, Chicago, IL 60607, United States

<sup>4</sup>Department of Chemistry and Nanoscience Center, University of Jyväskylä, P.O. Box 35 FI-40014 Jyväskylä, Finland

\* Authors to whom all correspondence should be addressed:  
Lvukov1@gmail.com, gerrit.x.groenhof@jyu.fi

Electronic Supporting Information (ESI)

## Methods

In order to examine how the initial molecular degrees of freedom, coordinates and atomic velocities, affect the outcome of the (cis, trans) photoisomerization reaction, we prepare different initial configurations of the Schiff base (coordinates and velocities) on the  $S_0$  PES. Then, we vertically (photo-)excite these configurations to the  $S_1$  PES, and track their subsequent relaxation dynamics. The initial configurations are extracted from an *ab initio* molecular dynamics (MD) trajectory of the molecule on  $S_0$  (vacuum), simulated at  $T = 300$  K, using a stochastic dynamics integrator. We also simulate initial PSB2 conformations obtained through excitation of its individual normal modes and thermal ensembles with constrained dihedral angles.

We describe the PSB2 molecule by the complete active space self-consistent field (CASSCF) method in all the performed simulations. CASSCF is a multi-configuration method [1, 2]. In CASSCF, a judicious set of occupied and virtual orbitals is chosen, the so-called active-space orbitals. In this active space, a full configuration interaction calculation is performed, while the other orbitals are being kept doubly occupied or empty in all configurations. The occupied orbitals are optimized such that the electronic energy of the state considered is minimal.

In the  $S_0$  simulations, aimed at obtaining the unbiased thermal ensemble at  $T = 300$  K, the molecule is described at the CASSCF(4,4)/3-21G level, the timestep is 1 fs, and the temperature coupling is  $\tau_t = 0.01$  ps (stochastic dynamics integrator). From the 0.5 ns trajectory, we extract  $\approx 500$  frames at 1 ps intervals, and vertically excite the selected configurations to  $S_1$ .

In preparing the pre-twisted ground state thermal ensembles, we harmonically restrain the selected dihedral angles of the molecule with a force constant of  $k_{dih} = 10,000$  kJ/mol/rad<sup>2</sup>. We run classical MD simulations (OPLS all atom force field [3]) on the restrained molecule, extract the frames at every 10 ps, and run these at CASSCF(4,4)/3-21G level for additional 0.5 ps each, prior to vertically exciting them to  $S_1$ , where the dihedral restraints are released.

In all the excited-state simulations, the molecular energy and momentum are preserved (no thermostat), and the molecule is described at the state averaged (SA2) CASSCF(4,4)/6-31G\* level of theory. The timestep is set to 0.5 fs. The excited molecule, initially promoted to the  $S_1$  PES, relaxes towards the conical intersection (CI) seam, where it “hops” to the ground state. We compare the results of the photo-induced reaction using two hopping algorithms, the fewest switches hopping (FSH) algorithm [4] and the diabatic surface hopping (DSH) algorithm [5]. The ground and excited state simulations are performed using the GROMACS 4.0 [6] interface to Gaussian03 [7] and a development version of the GROMACS 4.0 interface to MOLPRO [8]. The GROMACS/MOLPRO interface with the fewest switches surface hopping algorithm [4] code is available upon request. We evaluated the excited state lifetimes in the photo-excited ensembles by fitting the  $S_1$  population to  $e^{-t/\tau}$ . In all the fitting procedures, we used the data points for the  $S_1$  population in the time interval  $t = 0 - 500$  fs. We used the same time interval in all the fitting procedures because we noticed that fit results are sensitive to the interval length (in all the analyses,  $S_1$  population is equal to zero long before 500 fs after the photo-excitation).

In Fig. 1, we show the CAS active space molecular orbitals for the  $S_1$  ( $S_0$  similar) state of a representative initial geometry. The  $\pi_1$ ,  $\pi_2$ ,  $\pi_3^*$  and  $\pi_4^*$  CAS orbitals are occupied with  $\approx 2e, 2e, 0e$  and  $0e$  and  $\approx 2e, 1e, 0e$  and  $1e$  on the  $S_0$  and  $S_1$  PES, respectively.

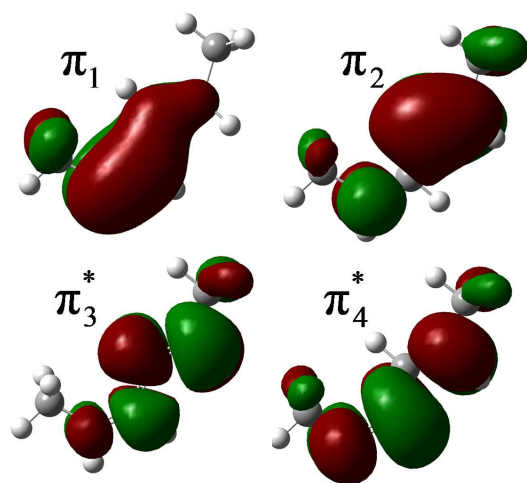


Figure 1: CAS active space molecular orbitals for the  $S_1$  state of a representative initial geometry.

### Energy profiles of $S_0$ , $S_1$ and $S_2$ electronic states in PSB2

We examined the characters of the  $S_0$ ,  $S_1$  and  $S_2$  states along the reaction pathways observed in the molecular dynamics simulations, i.e. changes of dihedrals around the  $N_2C_3$  and  $C_4C_5$  bonds, starting from the Franck-Condon geometries and ending at the conical intersection geometries.  $S_1$  and  $S_2$  states are the  $1B_2$  (ionic) and  $2A_1$  (covalent) states, respectively. Our results, shown in Figs. 2 and 3, show that ordering of the  $S_1$  and  $S_2$  states is preserved along the two tested reaction pathways.

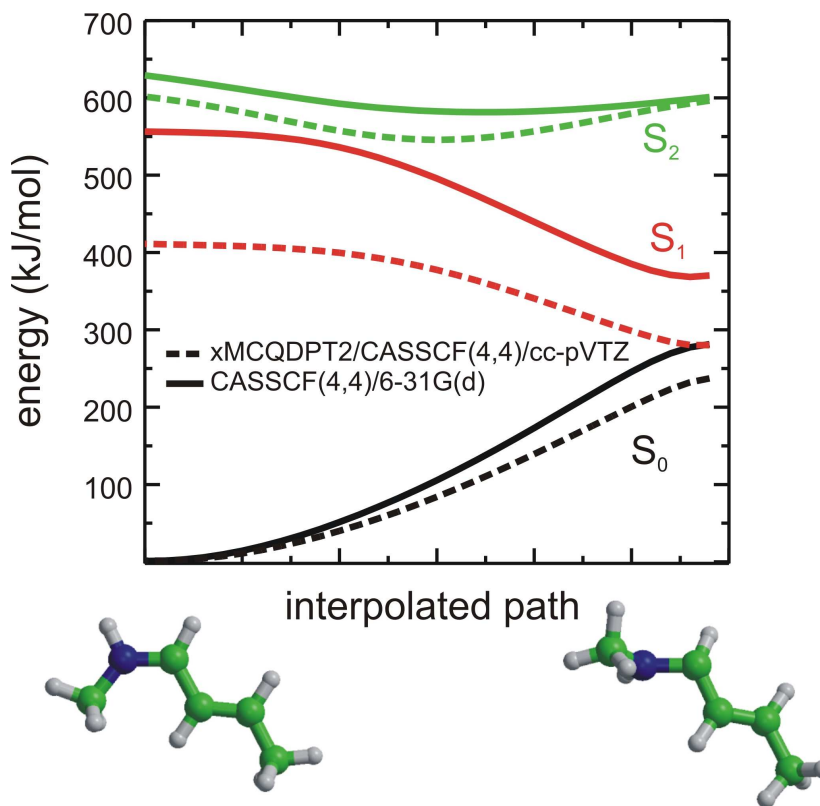


Figure 2: Potential energy profiles of the  $S_0$ ,  $S_1$  and  $S_2$  electronic states along the linearly interpolated pathway between the planar  $S_1$  minimum and the  $N_2=C_3$  twisted  $S_1/S_0$  conical intersections. Note that because the curves were obtained using state-averaged orbitals for the three electronic states, whereas the CI geometry was obtained using only ground and first excited states, the degeneracy is lifted. Continuous lines are SA3-CASSCF(4,4)/6-31G(d) energies without dynamic electron-electron correlation. Dashed lines are xMCQDPT2/CASSCF(4,4)/cc-pVTZ energies [9]

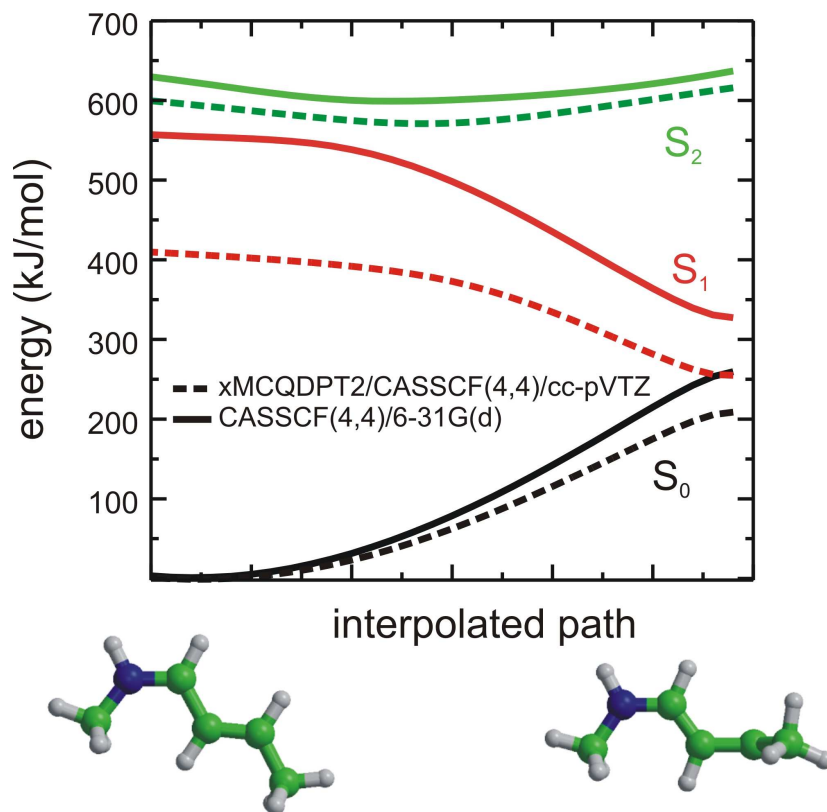


Figure 3: Potential energy profiles of the  $S_0$ ,  $S_1$  and  $S_2$  electronic states along the linearly interpolated pathway between the planar  $S_1$  minimum and the  $C_4=C_5$  twisted  $S_1/S_0$  conical intersections. Note that because the curves were obtained using state-averaged orbitals for the three electronic states, whereas the CI geometry was obtained using only ground and first excited state, the degeneracy is lifted. Continuous lines are SA3-CASSCF(4,4)/6-31G(d) energies without dynamic electron-electron correlation. Dashed lines are xMCQDPT2/CASSCF(4,4)/cc-pVTZ energies [9].

### Energy profiles for rigid rotation of the $\text{CN}_2\text{C}_3\text{C}$ and $\text{CC}_4\text{C}_5\text{C}$ dihedrals in PSB2

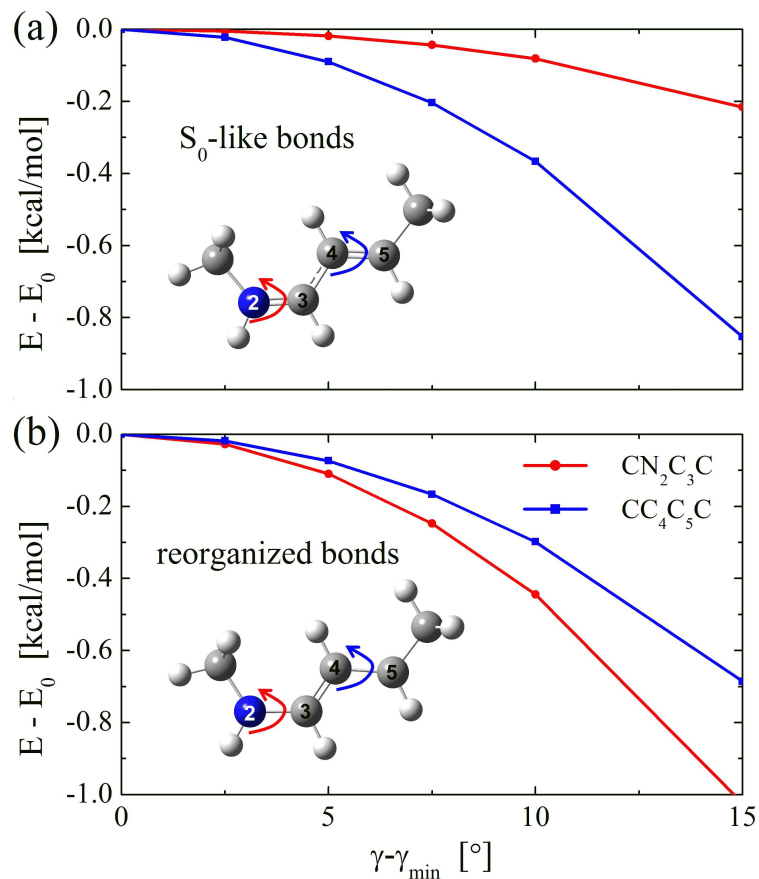


Figure 4: (a) Energy profiles on the  $S_1$  surface for rigid rotation of the  $\text{CN}_2\text{C}_3\text{C}$  and  $\text{CC}_4\text{C}_5\text{C}$  dihedrals for nuclear positions of the  $S_0$  state, which are preserved in the  $S_1$  state, immediately upon vertical excitation. (b) Same as in (a), for the molecule with the nuclear positions of the  $S_1$  state, which develops within 15 – 20 fs after excitation during the dynamics simulations. To obtain the  $S_1$  molecular geometry for the planar molecule, we optimize the molecule geometry on  $S_1$ , starting with the geometry at the  $S_0$  minimum ( $\gamma_{\min}$ ) and holding the dihedral angles which keep the molecular frame planar fixed. The molecule is described within SA2-CAS(4,4)/6-31G\* level of theory, as in the simulations.

## Diabatic surface hopping

Here we describe the basic assumptions behind the diabatic surface hopping algorithm. This algorithm is described in greater detail in [5, 10]. The diabatic hopping algorithm is based on the one-dimensional Landau-Zener equation, which relates the probability of a transition between two electronic states  $\Psi_2$  and  $\Psi_1$  to the nonadiabatic coupling, via

$$P_{2 \rightarrow 1} = \exp\left(-\frac{1}{4}\pi\xi\right) \quad (1)$$

In this equation  $\xi$  is the Massey parameter, defined as

$$\xi = \frac{\Delta E}{\hbar \frac{dQ}{dt} g(Q)}, \quad (2)$$

where  $\Delta E$  is the energy gap between the adiabatic states,  $Q$  represents a one dimensional nuclear reaction coordinate, and

$$g(Q) = \langle \Psi_1 | \nabla_Q \Psi_2 \rangle \quad (3)$$

is the derivative coupling vector. If we differentiate  $\Psi_2$  with respect to  $t$  via  $\frac{dQ}{dt}$ , we can rewrite  $\xi$  as

$$\xi = \frac{\Delta E}{\hbar \langle \Psi_1 | \frac{d\Psi_2}{dt} \rangle}. \quad (4)$$

To decide when to undergo a transition to a different potential energy surface, one would in principle need to compute  $\langle \Psi_1 | \frac{d\Psi_2}{dt} \rangle$  at every time step ( $\Delta t$ ) of the simulation. In practice, however, it is possible to approximate the derivative coupling vector  $\langle \Psi_1 | \frac{d\Psi_2}{dt} \rangle$  as  $\langle \Psi_1(t) | \Psi_2(t + \Delta t) \rangle$ , i.e., the overlap between the excited-state wave function at the current time step and the ground-state wave function at the previous time step. Since in our simulations we use the complete active space self-consistent field (CASSCF) method with state-averaged (SA) orbitals to model the wave function, we compute the overlap as the inner product of the corresponding SA-CASSCF eigenvectors  $C_1$  and  $C_2$ :

$$\langle \Psi_1(t) | \Psi_2(t + \Delta t) \rangle = C_1^t \cdot C_2^{t+\Delta t}. \quad (5)$$

Calculating the energy gap  $\Delta E$  and  $C_1^t \cdot C_2^{t+\Delta t}$  at every time step is straightforward, and we can use the Landau-Zener formula to calculate the probability of a transition to the other surface. In principle, the transition probability can be used to spawn a new trajectory on the other surface. However, since this procedure would lead to multiple trajectories that have to be computed simultaneously, spawning is too demanding in practice. We therefore restrict hopping to situations where the transition probability approaches unity. This happens at the conical intersection seam, where  $\Delta E \approx 0$  and  $C_1^t \cdot C_2^{t+\Delta t} \approx 1$ .

Because we allow hopping only at the conical intersection seam, our classical trajectories never leave the diabatic surface. Therefore, energy and momentum are obviously conserved. In principle, this strict diabatic hopping criterion could lead to an underestimation of the population transfer probability, because a surface hop in regions with strong non-adiabatic coupling far from the intersection is prohibited. In practice, however, the high dimensionality of the seam ensures that all trajectories encounter such regions of high transfer probability. A major advantage of restricting hopping to the seam is that we obtain information on the location of the seam in our trajectories. The latter is important to understand how the interactions between a chromophore and its (protein) environment alter the topology of the surfaces and the seam and thereby control the outcome of the photochemical process. The Landau-Zener model is clearly an approximation, but can help to keep a proper physical insight, which is crucial for understanding complex systems.

## Atomic Displacements along Normal Modes in Internal Coordinates

Here, we describe our calculations and numerical approximations used to obtain the atomic displacements along the normal modes in the basis of non-redundant internal coordinates of the PSB2 molecule. In all the calculations we used Gaussian03 [7]. We performed frequency calculations on the PSB2 molecule on the  $S_0$  PES, optimized at the CASSCF/6-31G\* level of theory, to obtain atomic displacements of the molecule along its  $m = 42$  normal modes. The modes are expressed in the Cartesian coordinates,  $\vec{N}_{m, \text{cart}}$  ( $\vec{N}_{m, \text{cart}} \vec{N}_{m, \text{cart}} = 1$ ). Since some of the normal mode displacements involve rotations, we express all the modal displacements in curvilinear non-redundant internal coordinates of the molecule. Several of the “rotation” modes have low frequencies and large displacements at the room temperature (not suitably described by  $\vec{N}_{m, \text{cart}}$ ).

In order to find out how normal modes are populated in arbitrary configurations of the molecule (thermal ensemble), we first need to describe small perturbations of the molecule along the normal modes in the internal coordinates. We prepare a set of PSB2 structures,  $\vec{R}_{m, \text{cart}}$ , by slightly distorting the minimum energy geometry,  $\vec{R}_{0, \text{cart}}$ , along each of the 42 normal modes,

$$\vec{R}_{m, \text{cart}} = \vec{R}_{0, \text{cart}} + k_m \vec{N}_{m, \text{cart}}, \quad m = 1, \dots, 42, \quad (6)$$

where we choose a small value of  $k_m = 0.03$ . We project the vectors  $\vec{R}_{m, \text{cart}}$  onto a set of non-redundant internal coordinates (the default set in Gaussian calculations)  $\vec{R}_{m, \text{int}}$ . This gives us the normal mode displacements in these internal coordinates,

$$k_m \vec{N}_{m, \text{int}} \approx \vec{R}_{m, \text{int}} - \vec{R}_{0, \text{int}}, \quad (7)$$

where  $\vec{R}_{0, \text{int}}$  is the minimum energy PSB2 geometry, expressed in the non-redundant internal coordinates. We use the vectors  $\vec{N}_{m, \text{int}}$  to perform a normal mode analysis to obtain the unknown  $k_m$  coefficients.

In Fig. 5 (a-c), we show the energy of the molecule,  $E$ , calculated by Gaussian03, in dependence of the displacement,  $k_m$ , along the 1, 2 and 5 modes. Two separate sets of structures are prepared, when these  $k_m$  are used in the Cartesian and the internal coordinates. Here,  $E = E_{\text{displ}} - E_0$ , where  $E_{\text{displ}}$  is the energy of a molecule with atoms displaced along the normal mode  $m$  and  $E_0$  is the minimum energy. We also present a quadratic approximation for the energy ( $E = c_m (k_m \vec{N}_m)^2 = c_m k_m^2$ ), when the constant  $c_m$  is extrapolated from the energies of the molecular structures displaced along  $\vec{N}_{m, \text{cart}}$  at  $k_m = 0.03$ . At small displacements, the three  $E$ -curves are very similar. At larger displacements, the energies associated with  $\vec{N}_{m, \text{cart}}$  largely deviate from those associated with  $\vec{N}_{m, \text{int}}$  and the quadratic fit. This plot shows that our numerical approximation (Eqs. 6 and 7) leads to a quadratic-like dependence for energies associated with  $\vec{N}_{m, \text{int}}$ .

We also test the energy additivity for different normal modes described by the internal coordinates. In Fig. 5 (d), we compare the energies ( $E_{\text{structure}}$ ) of molecules displaced along several normal modes, with those ( $E_{\text{predicted}}$ ) obtained by summing the energy contributions arising from displacements along the individual normal modes. We can see a good agreement between  $E_{\text{structure}}$  and  $E_{\text{predicted}}$ , confirming the validity of our numerical approximation (Eqs. 6 and 7).

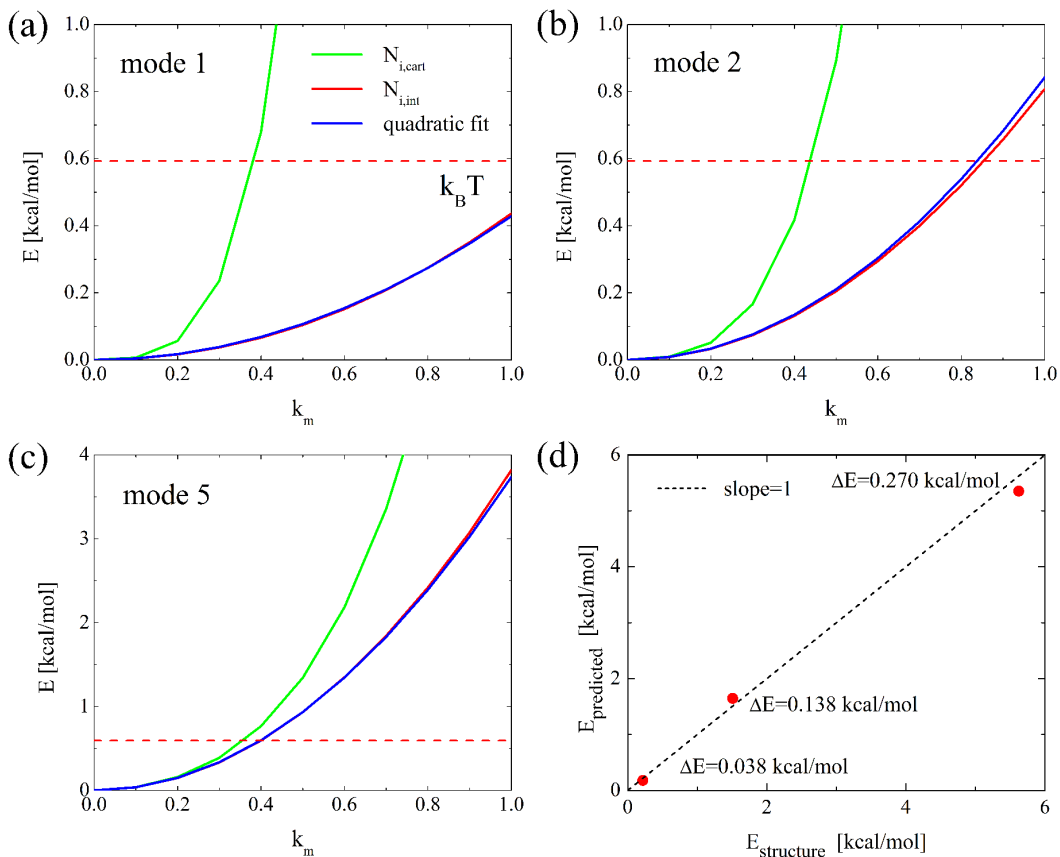


Figure 5: (a) Energies of the PSB2 molecules displaced along the normal mode 1 by the coefficient  $k_m$ . We compare the energies of PSB2 structures  $\vec{R}_{\text{cart}} = R_{0, \text{cart}} + k_m \vec{N}_{m, \text{cart}}$  and  $\vec{R}_{\text{int}} = R_{0, \text{int}} + k_m \vec{N}_{m, \text{int}}$ , where  $\vec{N}_{m, \text{cart}}$  are obtained from Gaussian calculation, and  $\vec{N}_{m, \text{int}}$  are approximated as shown in Eqs. 6 and 7. These energy profiles are compared with the energy expressed as a quadratic function of  $k_m$ , as described in the text. The dashed red line marks  $k_B T$ . (b) Same for mode 2 and (c) mode 5. (d) Comparison of predicted energies and calculated energies of several PSB2 geometries, when multiple normal modes are excited (the 3 cases have the (1-3), (1-6) and (1-9) modes excited). The excitation coefficients for the first point (closest to the origin) are  $k_{m=1-3} = 0.2, 0.2, 0.2$ , for the second point are  $k_{m=1-6} = 0.6, 0.5, 0.2, 0.3, 0.3, 0.2$ , and for the third point are  $k_{m=1-9} = 1.0, 0.9, 0.4, 0.5, 0.4, 0.2, 0.2, 0.1, 0.1$ . For the third point, we choose the coefficients to approximately give each excited mode the thermal energy  $k_B T$ . We show that the larger the number of the excited modes, and the larger the extension coefficient  $k_m$ , the more  $E_{\text{structure}}$  deviates from  $E_{\text{predicted}}$ .

**PSB2 geometry at the S<sub>0</sub> minimum (CASSCF(4,4)/6-31G\*)**

N	0.000000	0.000000	0.000000
H	0.000000	0.000000	1.002419
C	1.147986	0.000000	-0.583519
H	2.004300	-0.000052	0.067142
C	1.359127	0.000086	-2.009223
H	0.509029	0.000246	-2.665606
C	2.617621	-0.000078	-2.498291
H	3.444093	-0.000241	-1.805690
C	-1.322139	0.000142	-0.653957
H	-1.424688	-0.887660	-1.259616
H	-2.072889	-0.000213	0.119265
H	-1.424830	0.888381	-1.258956
C	2.969439	-0.000079	-3.952364
H	3.568873	0.873201	-4.188291
H	3.568665	-0.873486	-4.188349
H	2.090321	0.000048	-4.583737

## References

- [1] Siegbahn, P. E. M.; Almlöf, J.; Heiberg, A.; Roos, B. O. The complete active space SCF (CASSCF) method in a Newton–Raphson formulation with application to the HNO molecule. *J. Chem. Phys.* **1981**, *74*, 2384–2396.
- [2] Roos, B. O. Theoretical Studies of Electronically Excited States of Molecular Systems Using Multiconfigurational Perturbation Theory. *Acc. Chem. Res.* **1998**, *32*, 137–144.
- [3] Jorgensen, W. L.; Maxwell, D. S.; Tirado-Rives, J. Development and Testing of the OPLS All-Atom Force Field on Conformational Energetics and Properties of Organic Liquids. *J. Am. Chem. Soc.* **1996**, *118*, 11225–11236.
- [4] Tully, J. Molecular Dynamics with Electronic Transitions. *J. Chem. Phys.* **1990**, *93*, 1061–1071.
- [5] Fabiano, E.; Groenhof, G.; Thiel, W. Approximate Switching Algorithms for Trajectory Surface Hopping. *Chem. Phys.* **2008**, *351*, 111–116.
- [6] Spoel, D. V. der ; Lindahl, E.; Hess, B.; Groenhof, G.; Mark, A. E.; Berendsen, H. J. C. . *J. Comp. Chem.* **2005**, *26*, 1701–1718.
- [7] Frisch, M. J.; Trucks, G. W.; Schlegel, H. B.; Scuseria, G. E.; Robb, M. A.; Cheeseman, J. R.; Montgomery, J. A.; Jr., ; Vreven, T.; Kudin, K. N.; Burant, J. C.; Millam, J. M.; Iyengar, S. S.; Tomasi, J.; Barone, V.; Mennucci, B.; Cossi, M.; Scalmani, G.; Rega, N.; Petersson, G. A.; Nakatsuji, H.; Hada, M.; Ehara, M.; Toyota, K.; Fukuda, R.; Hasegawa, J.; Ishida, M.; Nakajima, T.; Honda, Y.; Kitao, O.; Nakai, H.; Klene, M.; Li, X.; Knox, J. E.; Hratchian, H. P.; Cross, J. B.; Bakken, V.; Adamo, C.; Jaramillo, J.; Gomperts, R.; Stratmann, R. E.; Yazyev, O.; Austin, A. J.; Cammi, R.; Pomelli, C.; Ochterski, J. W.; Ayala, P. Y.; Morokuma, K.; Voth, G. A.; Salvador, P.; Dannenberg, J. J.; Zakrzewski, V. G.; Dapprich, S.; Daniels, A. D.; Strain, M. C.; Farkas, O.; Malick, D. K.; Rabuck, A. D.; Raghavachari, K.; Foresman, J. B.; Ortiz, J. V.; Cui, Q.; Baboul, A. G.; Clifford, S.; Cioslowski, J.; Stefanov, B. B.; Liu, G.; Liashenko, A.; Piskorz, P.; Komaromi, I.; Martin, R. L.; Fox, D. J.; Keith, T.; Al-Laham, M. A.; Peng, C. Y.; Nanayakkara, A.; Challacombe, M.; Gill, P. M. W.; Johnson, B.; Chen, W.; Wong, M. W.; Gonzalez, C.; Pople, J. A. Gaussian 03, Revision C.02. *Gaussian, Inc., Wallingford* **2004**.
- [8] Werner, H. J.; Knowles, P. J.; Lindh, R. *MOLPRO, version 2009.1.* **2009**.
- [9] Granovsky, A. A. Extended multi-configuration quasi-degenerate perturbation theory: The new approach to multi-state multi-reference perturbation theory. *J. Chem. Phys.* **2011**, *134*, 214113–14.
- [10] Groenhof, G.; Boggio-Pasqua, M.; Schäfer, L. V.; Robb, M. A., *Combining Quantum Mechanics and Molecular Mechanics. Some Recent Progresses in QM/MM Methods*, Sabin, J. R.; Brändas, E., eds. (Academic Press, 2010), vol. Volume 59, pp. 181–212.